Acoustic add-drop filters based on phononic crystal ring resonators

Babak Rostami-Dogolsara,[1] Mohammad Kazem Moravvej-Farshi,[1,*] and Fakhroddin Nazari[2]
[1]*Faculty of Electrical and Computer Engineering, Tarbiat Modares University, P. O. Box 14115–194, Tehran 1411713116, Iran*
[2]*Faculty of Engineering Modern Technologies, Amol University of Special Modern Technologies, Amol 4616849767, Iran*
(Received 6 July 2015; revised manuscript received 28 November 2015; published 15 January 2016)

We report the design procedure for an acoustic add-drop filter (ADF) composed of two line-defect waveguides coupled through a ring resonator cavity (RRC) all based on a phononic crystal (PnC) platform. Using finite difference time domain and plane wave expansion methods, we study the propagation of acoustic waves through the PnC based ADF structures. Numerical results show that the quality factor for the ADF with a quasisquare ring resonator with a frequency band of 95 Hz centered about 75.21 kHz is $Q \sim 800$. We show that the addition of an appropriate scatterer at each RRC corner can reduce the scattering loss, enhancing the quality factor and the transmission efficiency. Moreover, it is also shown that by increasing the coupling gaps between the RRC and waveguides the quality factor can be increased by ∼25 times, at the expense of a significant reduction in the transmission efficiency this is attributed to the enhanced selectivity in expense of weakened coupling. Finally, by varying the effective path length of the acoustic wave in the RRC, via selectively varying the inclusions physical and geometrical properties, we show how one can ultra-fine and fine-tune the resonant frequency of the ADF.

DOI: 10.1103/PhysRevB.93.014304

I. INTRODUCTION

Heterogeneous materials with periodic structures known as phononic crystals (PnCs) have attracted a great deal of researchers' attentions in recent years [1–3]. A PnC is a man-made crystal composed of two or more different acoustic materials arranged in a periodic manner to control the propagation of a specific mechanical wave [4–6]. There are numerous potential applications such as acoustic couplers [7], lenses [8,9], waveguide [10,11], demultiplexer [12], and switches [13] for PnCs.

High-Q cavity is an important part of most PnC-based acoustic devices such as acoustic filters [14,15], sensors [16,17], and sources [18,19]. Eigenmodes of a cavity can be used advantageously to induce either narrow passing bands within the stop band of a PnC or very narrow stopping bands in the pass band of a waveguide. By exciting a specific resonant mode in a cavity, the wave amplitude can be amplified significantly. Thus, a PnC-based cavity may serve as an acoustic source. Hence, high-Q cavities made on PnC platforms can play a key role in developing micromechanical resonators [20]. By demonstrating an acoustic channel drop tunneling in a PnC platform, the possibility of transferring one particular acoustic wavelength between two parallel PnC waveguides coupled through an appropriate coupling element was recently investigated [21]. The coupling element was composed of two coupled point defect cavities interacting with stubs located at the sides of the two parallel guides. The transmission peak and quality factor obtained from the coupling in this structure are not good enough and need to be improved by new design.

Microresenators based on PnC structures, specifically PnC-based ring resonators have been shown to exhibit high quality factors, reducing energy losses [22–24]. To enhance the cavity quality factor and transmission efficiency, in this paper, we have taken the advantage of a ring resonator as the cavity and coupling element. While the acoustic wave is circulating in a PnC-based ring resonator cavity (RRC), the resonance phenomenon amplifies the wave amplitude in the cavity. We show that a PnC-RRC due to its multimode nature, offers scalability in size and flexibility in mode design, as compared to the point-defect resonator used by Pennec *et al.* [21]. By using this type of cavity, we propose a PnC-based add-drop filter (ADF) that can be used as a building block of acoustic add-drop multiplexers, switches, filters, as well as temperature and liquid's molality sensors. The proposed PnC-ADF consists of two line-defect PnC waveguides coupled via a single PnC-RRC, with high wavelength selectivity. Similar ADF structures based on photonic crystal platforms have been used for optical applications [25]. Although PnC and photonic crystals (PhC) based devices have many common characteristics, they also have significant differences. (i) When an acoustic or elastic wave propagates within a perfectly ordered fluid or solid, coherent and collective movements of molecules or atoms take place. This makes the nature of the acoustic/elastic wave propagation different from that of the electromagnetic wave, in a medium that interacts with the matter through its constituent atoms. (ii) The transverse components of sound waves cannot propagate in any fluid/fluid PnC-based device. In other words, only the longitudinal component of a sound wave can propagate in such a PnC-based device. This is, however, not true for a similar PhC-based device through which transverse electric (TE) or transverse magnetic (TM) polarized optical signals can propagate. For example, in the present case, when a uniform acoustic pressure (plane wave) with a center frequency, coinciding with the vibrating frequency of the molecules of the ring resonator constituents, is applied to the medium the molecules of the background material (i.e., Hg in the present case) start vibrating longitudinally (i.e., perpendicular to the water rods) with the same acoustic frequency. Hence, this acoustic mode can be selected by the ring resonator and thus the PnC-ADF can function. On the other hand, for a similar PhC-ADF to function one needs to couple an optical signal of desired polarization

*Author to whom correspondence should be addressed: Farshi_k@modares.ac.ir

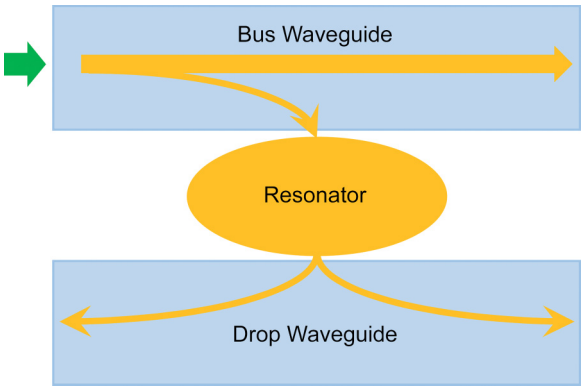

FIG. 1. Schematic of a generic resonant-cavity add-drop filter.

with a designed frequency, to the ADF input port within a specific cone.

In this investigation we show that, by devising appropriate scatterers at four corners of the quasisquare RRC, its Q factor and coupling efficiency can be enhanced.

II. PROPOSED PnC-ADF STRUCTURE

A general schematic of a RRC-based ADF is shown in Fig. 1. It consists of two waveguides, the bus and the drop, coupled to each other through an RRC. When a multifrequency signal propagates along the bus waveguide, a single frequency channel, whose center frequency satisfies the RRC resonance condition, will be selected by the RRC and transferred out of the bus and into the drop waveguide, either in the forward or backward propagation direction.

The proposed PnC-RRC ADF, in this work, is based on a two-dimensional (2D) square lattice PnC structure, consisting of a periodic array of fluidic (water) rods of radii r as inclusions with the periodicity of a embedded in a mercury background. PnC-based devices, using similar choices of constitutive materials (i.e., fluid-fluid) have already been practically realized [26–28]. As explained in all these references, a thin solid shell should separate the inclusions' and background's fluids to maintain a stable fluid-fluid PnC, in practice. Moreover, by comparing the experimental and theoretical results it has been shown that the effect of the thin solid shell on device operation can be neglected [26,28]. The volume mass densities for the inclusions and the background are $\rho_A = 998\,\mathrm{kg/m^3}$ and $\rho_B = 13545\,\mathrm{kg/m^3}$, wherein the sound wave propagates longitudinally with speeds of $c_{LA} = 1490\,\mathrm{m/s}$ and $c_{LB} = 1450\,\mathrm{m/s}$, respectively. In this investigation, the fill fraction is taken to be $ff = \pi r^2/a^2 = 0.3$. This choice of fill fraction can easily be shown to provide the nearly maximum first phononic bandgap (PnBG).

Before going any further, we present the band structure and transmitivity of a perfect PnC and a line-defect PnCW, calculated as done by Khelif *et al.* [14,15]. Figure 2(a) illustrates a 2D schematic of a line-defect PnCW that is made by removal of a column of rods from a perfect squared lattice PnC of constant $a = 9$ mm. Dispersion curves versus the Bloch wavevector along the Γ-X direction and the transmission spectra of the perfect PnC are calculated using the plane-wave expansion (PWE) and finite difference time domain (FDTD) methods, as illustrated by the dashed curves in Figs. 2(b) and 2(c), respectively. The associated PnBG is also depicted by the shaded area in Fig. 2(b). Using the supercell, represented by the rectangle encompassed by the dashes in Fig. 2(a), and employing the PWE the dispersion curves of the line-defect PnC waveguide along the Γ-X direction are calculated and shown by the solid curves in Fig. 2(b). The transmission spectrum through the line defect PnC waveguide, obtained by FDTD method, is also shown by the solid cure in Fig 2(c). Among the waveguide modes (the solid curves located within the PnBG), the upper one near the PnBG edge weakly interacts with the nearest bulk mode, folding at the crossing point that results in a small secondary gap of ∼95 kHz near the edge of the Brillouin zone (BZ). On the contrary, the lower mode is far enough from the PnBG edge to interact with the bulk modes and is suitable for practical guiding applications. The dispersion relation for this guided mode, over the entire BZ except around its edge, can be well approximated by a parabolic relation similar to that of a guided mode in a waveguide with perfect reflecting walls [14],

$$f^2 = f_T^2 + c_m^2 (k/2\pi)^2,$$

where f, k, and c_m are the sound frequency, wave vector, and velocity in mercury, and

$$f_T = c_m/2d$$

can be considered as the cutoff frequency in the PnBG region associated with a waveguide of effective width d. For the

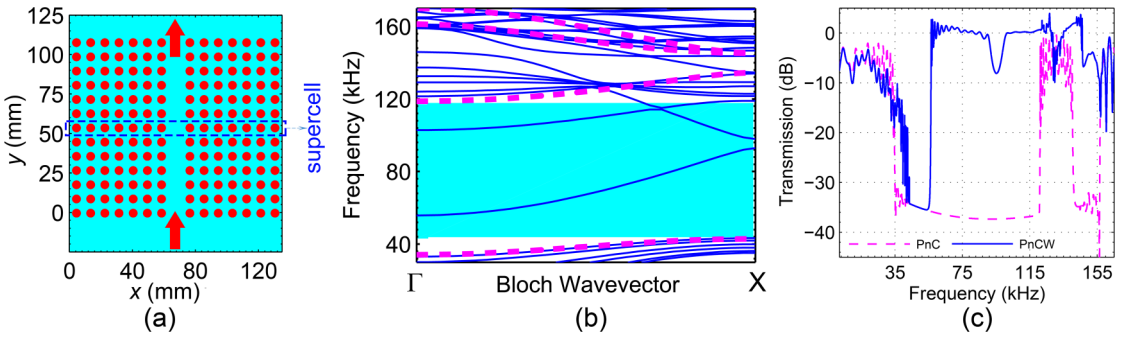

FIG. 2. (a) 2D schematic of line-defect PnC waveguide based on square lattice of period a. (b) Dashes and shaded region show the band structure and the first PnBG of the perfect PnC with $ff = 0.3$, and solid curves show the dispersion curves for the line-defect PnC waveguide. (c) Transmission spectra through the perfect PnC (- - -) and the line-defect PnC waveguide (——).

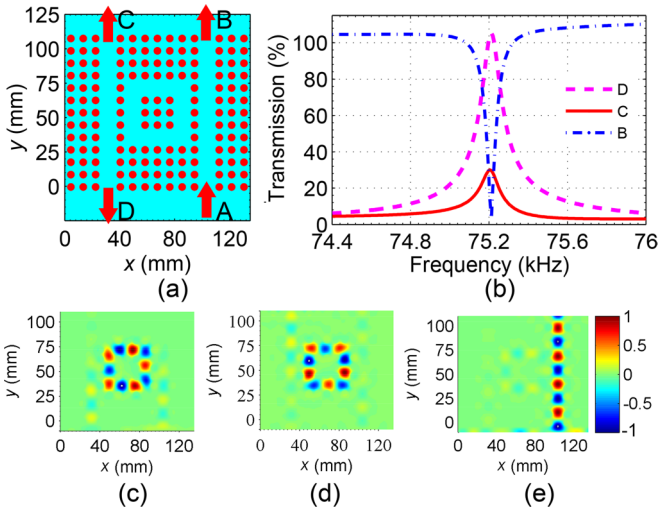

FIG. 3. (a) Schematic top view and (b) transmission spectra through the output ports B, C, and D (the dropping scenario) of the PnC-ADF. The pressure distributions for the RRC's (c) dropping and (d) adding scenarios for the resonant mode of 75.21 kHz entering from ports A and C, respectively. (e) The pressure distribution for the nonresonant acoustic wave of frequency 74.5 kHz, entering from port A.

PnC waveguide example of Fig. 2, with $d = 12.6$ mm and $f_T = 57$ kHz, the frequency range of interest for simulation falls within $56\,\text{kHz} < f < 93\,\text{kHz}$. It is worth noting that the waveguide transmittance is calculated by averaging the pressure amplitude over its output port cross section normal to the guide axis, and then normalizing its Fourier transform to the similar quantity evaluated for the same acoustic wave propagating through the same background material with no inclusions (water rods). This procedure has resulted in maximum transmission values in excess of unity, as can be seen in Fig. 2(c). Similar observations have been reported by others [12,14,15,26] who used the same technique in calculating the transmittance for their PnC waveguides.

Figure 3(a) depicts a 2D (top) schematic view of a four-port ADF based on PnC-RRC, described at the opening of Sec. II. As shown in this figure, two line-defect PnC waveguides are coupled through a PnC-RRC that is formed by removal of rods from the perimeter of a 5×5 square from the middle. The ADF facing ports in the bus and drop waveguides are labeled as A and D, while the corresponding nonfacing ports are labeled B and C, respectively. A wide band Gaussian acoustic pulse, covering the frequency range of interest, is launched into facing port A of the bus waveguide. The RRC selects and drops a narrow band, from the input, whose center frequency satisfies the resonant condition of $f = Nc_m/L$, with $N = 1, 2, 3, \ldots$, and L is the ring average perimeter. This particular narrow band acoustic wave after being amplified in the RRC is coupled into the drop waveguide and then is transmitted out of its facing port D. However, the remaining acoustic band transmits out of the nonfacing port B and C of the bus and drop waveguide, respectively. This criterion is called as wavelength dropping. In this case, the propagation of this particular acoustic mode within the RRC is counterclockwise. On the other hand, when the same wide band Gaussian acoustic pulse is launched into the nonfacing port C of the drop waveguide, as a consequence of which the same narrow acoustic band is selected and amplified by the RRC, and then coupled to the bus waveguide and hence transmits out of its non-facing port B, the adding criterion is prevailed. For this criterion the propagation through the RRC is also counterclockwise. It is worth mentioning that due to the structural symmetry of the proposed ADF, as observed from Fig. 3(a), the adding scenario implies the dropping scenario straightforwardly. Nevertheless, our emphasis on this issue to reiterate the main purpose of this paper that is to present the design of a single acoustic filter that can function as an drop-filter as well as a add-filter with a structure that differ from those that can solely function as a drop filter [14] or an add filter [15].

Employing the 2D FDTD numerical method and applying the absorbing boundary conditions at the outer boundaries, we simulated the transmission spectra through the ports B, C, and D as well as the profiles of the acoustic pressure throughout the ADF structure in the frequency range of interest. Notice that an absorbing boundary acts as an impedance-matched boundary through which an incoming wave passes without being reflected [11,29]. Figure 3(b) illustrates the transmission spectra of the selected acoustic band of 74.4 to 76 kHz, through the ports B, C, and D, for the dropping scenario. As shown in this figure, a very narrow band of $\Delta f = 95$ Hz, centered about $f_0 = 75.21$ kHz, is mainly dropped out by the nonfacing port D of the drop waveguide. In other words, the RRC's quality factor is $Q = f_0/\Delta f \approx 800$. Also shown in this figure, the partial dropping of the resonant mode from the facing port C of the drop waveguide. This is an undesirable phenomenon as is due to the significant scattering in the ring resonator resulting in a low drop efficiency and poor spectral selectivity. Figures 3(c) and 3(d) show the pressure distributions for the resonant acoustic mode through the RCC for the dropping and adding scenarios, respectively. Furthermore, Fig. 3(e) demonstrates the pressure distribution for a nonresonant mode centered about 74.5 kHz that being launched into the bus waveguide via its facing port, A, and without being coupled to the RRC is solely transmitted out of the bus waveguide through its nonfacing port B.

To increase the RRC's quality factor, the scattering losses due to the bends of the quasisquare ring should be reduced, by rearranging the scatterers there, appropriately. As can be observed in Fig. 4(a), we added a scatterer rod at each of the RRC's four corners. The radii and the mechanical properties of the new rods are the same as those forming the original PnC. They are each positioned at the center of their four nearest-neighboring rods—i.e., on the axis of the square constituting the RRC's outer boundary centered at the point $a\sqrt{2}/2$ away from the corner. Presence of these scatterer rods at the RRC's four corners suppresses the nonresonant modes by smoothing out the wave rotation path within the ring, as a result of which the output quality factor increases.

Figure 4(b) illustrates the transmission spectra for the dropping scenario, through the ports A, B, and C for the modified PnC-ADF, with an additional scatterer rod positioned at each of the RRC's four corners. As can be observed from this figure, the presence of an additional scatterer at each of the RCC's four corners, has improved the RRC's spectral selectivity, resulting in a $Q \approx 1700$. The new acoustic resonant

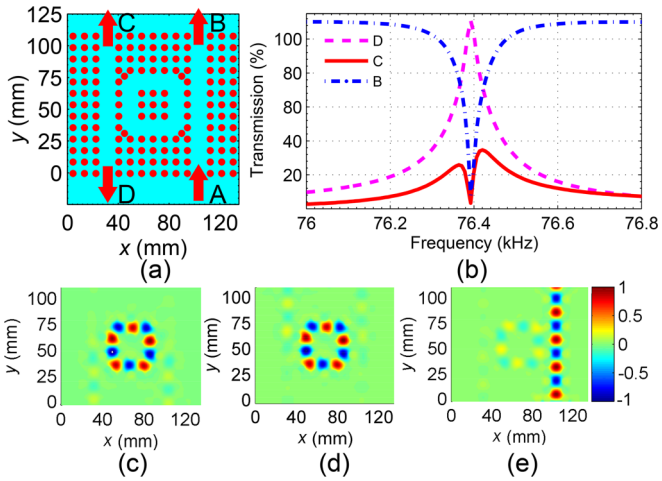

FIG. 4. (a) Schematic top view and (b) the transmission spectra through the output ports B, C, and D (the dropping scenario) of the modified PnC-ADF with four additional scatterer rods positioned at the RRC's four corners. The pressure distributions for the RRC's (c) dropping and (d) adding scenarios for the resonant mode of 76.39 kH, entering from ports A and C, respectively. (e) The pressure distribution for nonresonant acoustic wave of frequency 75.6 kHz, entering from port A.

mode exhibits a so-called "blue shift" of ∼1.18 kHz with a reduced bandwidth of $\Delta f = 44.94$ Hz. The so-called blue shift in the RRC's resonance frequency is a consequence of the effectively shortened acoustic wave path within the ring due to the presence of the four additional scatterers. In addition, these four additional scatterers also have caused a dip to appear in the transmission spectrum through the output port C, centered about the RRC's resonant frequency of $f_0 = 76.39$ kHz. This dip is also due to the presence of the four scatterers in the four corners of the RRC, enhancing the coupling strength between the RRC and the bus and drop waveguides, in effect. As a consequence, almost the entire input signal at the resonant frequency is selected by the RRC and then dropped to port D, leaving no chance for leakage through ports B and C. Snapshots of the distributions of the dropped and added cavity resonant mode, entering from ports A and C, are shown in Figs. 4(c) and 4(d), respectively. Figure 4(e) demonstrates the pressure distribution for the nonresonant acoustic wave of frequency 75.6 kH, entering from port A and exiting from port B.

To enhance the PnC-ADF quality factor further, one may increase the coupling gap between the line-defect waveguides and the RRC that in-turn decreases the coupling efficiency. In this regard, by adding an extra column of rods on each side of the RRC, we shifted the line-defect PnC waveguides away from the ring resonator on both sides, as can be observed from Fig. 5(a). The transmission spectra for the dropping scenario, through the output ports B, C, and D, when the acoustic wave enters through port A, is illustrated in Fig. 5(b). As can be deduced from this figure, although the quality factor for the PnC-ADF is increased beyond 20 000, its dropping efficiency is decreased considerably. This is because there is a trade-off between the quality factor Q and the coupling/dropping efficiency. In fact, adding an extra column of rods on each side

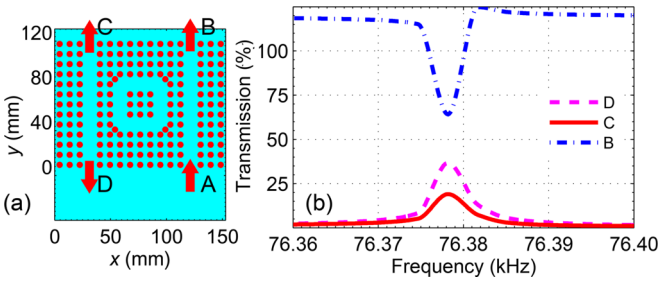

FIG. 5. (a) The schematic top view and (b) the transmission spectra for dropping scenario through the output ports B, C, and D of the modified PnC-ADF with increased coupling gap.

of the RRC has reduced the coupling coefficient between the RRC and the bus and the drop waveguides significantly. As a consequence of this, more than half of the input signal is leaked out through port B in the first place. In addition, for the same reason only about two-thirds of the resonant mode selected by the RRC that has been coupled to the drop waveguide is dropped out of port D; the reminder is leaked out through port C.

Any perturbation in dimension and/or mechanical properties of the rods in the structure is expected to change the characteristics of the PnC-ADF. Recently, an experimental study [30] showed that in aqueous binary mixtures of K_3PO_4, the mass density (ρ) and the sound velocity (c_L), at a given temperature depend on its molality. For example, Table I tabulates these dependencies at $T = 298.15$ K. At first, by adding K_3PO_4 to the water in the nine inner rods of the RRC with different molalities, we calculated the cavity resonant frequencies. The open circles in Fig. 6(a) show the numerical results for the molalities in the range of 0 to 0.9 as an example. By careful inspection one can find that the resonant frequency increases very slightly from 76.39–76.43 kHz as the aqueous molality varies from 0 to 0.9. This slight "blue shift" is due to the slight increase in the sound velocity of the mixture and hence the slight decrease in the "path length" that acoustic wave traverses through the RRC. These results are useful for ultrafine tuning of the resonant frequency. Next, we used the same aqueous mixtures in all rods composing the PnC and recalculated the resonant frequency versus the mixture molality. The numerical results are shown by the stars in Fig. 6(a). In this case, the variation in the mixture molality can act as a fine frequency tuning tool. This property can be used for designing PnC based sensors to determine the liquids molality, similar to those reported with different PnC devices [27,31].

TABLE I. Mass density (ρ) and sound velocity (c_L) of aqueous binary mixture of K_3PO_4 versus its molality (M) at $T = 298.15$ K [30].

M(mol.kg^{-1})	ρ(kg. m^{-3})	c_L(m. s^{-1})
0	1000	1496.70
0.5	1101	1602.98
0.7	1146	1658.80
0.9	1192	1716.63

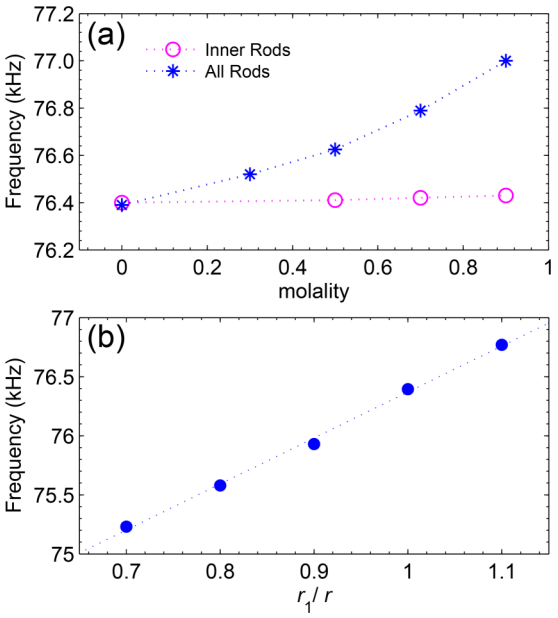

FIG. 6. Dependencies of the output resonance frequency on the (a) molality of the aqueous binary mixture in the (∘) inner rods only and entire rods (∗), and (b) relative changes in the radii of the inner rods.

Moreover, any variation in the rods radii also can change the resonant frequency. By varying the radii of the nine inner rods of the RRC, in the range of $0.7r \leqslant r_1 \leqslant 1.1r$, we calculated the resonant frequencies. The results are illustrated by the solid circles in Fig. 6(b). As can be observed from this figure, this variation also can act as a course tuning tool. In fact, as the ratio of r_1/r increases from 0.7 to 1.1, the resonant frequency increases linearly from 75.23 to 76.77 kHz. As the radii of the inner rods are increased, the RRC width is reduced effectively, causing the wavelength of the confined acoustic wave to decrease accordingly.

Furthermore, it was shown that variation in the temperature has different effects on the water and the mercury [32]; as an example Table II shows that the mass densities of mercury and water both decreases with an increase in the temperature, but with different rates. Nevertheless, while the sound velocity in the mercury decreases with an increase in its temperature, the

TABLE II. Mass densities (ρ) and sound velocities (c_L) of mercury and water at various temperatures (T) [32].

	ρ(kg. m^{-3})		c_L(m. s^{-1})	
T (°C)	mercury	water	mercury	water
0	13595	999	1460	1405
10	13570	999	1455	1447
20	13545	998	1451	1482
25	13545	997	1449	1497
40	13496	992	1442	1529
55	13460	986	1435	1547
60	13448	983	1432	1550
70	13423	977	1427	1555
80	13399	971	1423	1554

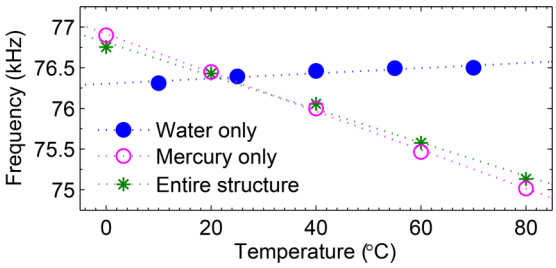

FIG. 7. Dependencies of the output resonance frequency on the temperature measured in water only (•) while background is kept at room temperature, mercury only when the water in rods are kept at room temperature (○), and the entire system is in equilibrium (∗).

sound velocity in water increases with the temperature. In this regard, first we kept the background temperature fixed at room temperature and solely varied the water temperature in the rods, assumed to be thermally isolated from the background. Then we calculated the resonant frequency, as depicted in the solid circles in Fig. 7. As can be observed from these results, the resonant frequency increases linearly with temperature with a small slope of 3.14 Hz/°C.

Next, we assumed the water temperature be kept fixed at room temperature and varied the background mercury temperature. The open circles in Fig. 7 illustrate the numerical results. As can be observed from these results, the resonant frequency in this case decreases linearly with the slope of −23.77 Hz/°C. The larger slope in this case is due to the fact that the acoustic wave is propagating mainly within the mercury. Finally, we kept the entire ADF in equilibrium and varied the temperature. The calculated numerical results are depicted by the stars in Fig. 7. The slope of the decrease in the resonant frequency for the case in equilibrium is ∼−19.7 Hz/°C. From the final results, one can conclude that thermal effect on the resonant frequency is dominated by the sound velocity in mercury. As the temperature increases, the sound velocity decreases and hence the acoustic wave path increases effectively. This property can be used for designing PnC based temperature sensors. Moreover, the results shown in Figs. 6 and 7 altogether demonstrate the possibility of designing a tunable acoustic ADFs.

III. CONCLUSION

Using a square lattice PnC structure composed a periodic array of water rods embedded in mercury background to design a new acoustic add-drop (ADF) filter. This PnC-ADF consists of two line-defects waveguide coupled through a square ring resonator (RRC), all on the aforementioned PnC platform. The PnC-RRC is formed by the removal of rods from the perimeter of a 5 × 5 square that is separated from the bus and drop waveguides by a column of rods on both sides. Using PWE and FDTD methods, we investigated PnBG and transmission spectra of the perfect PnC and the waveguides in response to acoustic waves. The numerical result shows that adding four scatterers with the same intrinsic properties as those of the original PnC, each at a corner of the RRC, increases backward-dropping efficiency by more than 5% and at the same time increases the quality factor by about more than two times.

Then, we studied the effect of the size of the coupling gap on the PnC-ADF characteristics. The numerical results show that the possibilities of achieving a high spectral selectivity with quality factor as high as Q ∼20 000 with the expense a significant reduction in the dropping efficiency. Then, by varying the physical properties of the fluidic scatterers inside the RRC by adding K_3PO_4 to the water with various molalities, we evaluated the resonant frequency verses the aqueous molality. The capability of ultrafine frequency tuning was demonstrated when only the content of the nine inner rods of the RRC were altered while the fine-tuning capability has been demonstrated by varying the properties of the entire rods forming the PnC-ADF structure. Moreover, by varying the radii of the nine inner rods, it has been shown that as the radii increase the RRC resonant frequency experiences a 385 Hz "blue shift" for every 10% increase in the radii of the inner rods with respect to those of the original rods, within the ring resonator. Finally, the effect of temperature on the dropping frequency has also been studied. Numerical results have shown that as the temperature of the entire constituents increase the dropping frequency exhibits the slope of −19.7 Hz/°C. This is attributed to the dominance of the sound velocity within the background mercury in response to the variation of the entire constituents' temperature. Nonetheless, if the water temperature is solely in changed the resonant center frequency experiences a relatively small positive slope of 3.14 Hz/°C.

ACKNOWLEGMENT

The authors would like to acknowledge the partial financial support, received from the Iran National Science Foundation (INSF).

[1] B. Graczykowski, M. Sledzinska, F. Alzina, J. Gomis-Bresco, J. S. Reparaz, M. R. Wagner, and C. M. Sotomayor Torres, Phys. Rev. B **91**, 075414 (2015).
[2] H. Lv, X. Tian, M. Y. Wang, and D. Li, Appl. Phys. Lett. **102**, 034103 (2013).
[3] R. Marchal, O. Boyko, B. Bonello, J. Zhao, L. Belliard, M. Oudich, Y. Pennec, and B. Djafari-Rouhani, Phys. Rev. B **86**, 224302 (2012).
[4] M. Sigalas and E. N. Economou, Solid State Commun. **86**, 141 (1993).
[5] M. S. Kushwaha, P. Halevi, L. Dobrzynski, and B. Djafari-Rouhani, Phys. Rev. Lett. **71**, 2022 (1993).
[6] F. R. Montero de Espinosa, E. Jiménez, and M. Torres, Phys. Rev. Lett. **80**, 1208 (1998).
[7] J.-H. Sun and T.-T. Wu, Phys. Rev. B **71**, 174303 (2005).
[8] A. Håkansson, J. Sánchez-Dehesa, and L. Sanchis, Phys. Rev. B **70**, 214302 (2004).
[9] S. Yang, J. H. Page, Z. Liu, M. L. Cowan, C. T. Chan, and P. Sheng, Phys. Rev. Lett. **93**, 024301 (2004).
[10] H. Chandra, P. A. Deymier, and J. O. Vasseur, Phys. Rev. B **70**, 054302 (2004).
[11] A. Khelif, P. A. Deymier, B. Djafari-Rouhani, J. O. Vasseur, and L. Dobrzynski, J. Appl. Phys. **94**, 1308 (2003).
[12] Y. Pennec, B. Djafari-Rouhani, J. O. Vasseur, A. Khelif, and P. A. Deymier, Phys. Rev. E **69**, 046608 (2004).
[13] R. Ganesh and S. Gonella, Phys. Rev. Lett. **114**, 054302 (2015).
[14] A. Khelif, B. Djafari-Rouhani, J. O. Vasseur, P. A. Deymier, Ph. Lambin, and L. Dobrzynski, Phys. Rev. B **65**, 174308 (2002).
[15] A. Khelif, B. Djafari-Rouhani, J. O. Vasseur, and P. A. Deymier, Phys. Rev. B **68**, 024302 (2003).
[16] A. Oseev, M. Zubtsov, and R. Lucklum, Procedia Engineering **47**, 1382 (2012).
[17] A. Oseev, M. Zubtsov, and R. Lucklum, Sens. Actuat. B **189**, 208 (2013).
[18] H. Sun and T. T Wu, IEEE Trans. Ultrason. Ferroelectr. Freq. Control **56**, 121 (2009).
[19] M. Ke, Z. Liu, P. Pang, W. Wang, Z. Cheng, J. Shi, X. Zhao, and W. Wen, Appl. Phys. Lett. **88**, 263505 (2006).
[20] S. Mohammadi, A. A. Eftekhar, R. Pourabolghasem, and A. Adibi, Sens. Actuat. A **167**, 524 (2011).
[21] Y. Pennec, B. Djafari-Rouhani, J. O. Vasseur, H. Larabi, A. Khelif, A. Choujaa, S. Benchabane, and V. Laude, Appl. Phys. Lett. **87**, 261912 (2005).
[22] D. Feng, D. Xu, G. Wu, B. Xiong, and Y. Wang, J. Appl. Phys. **115**, 024503 (2014).
[23] P. Boucher, S. Rauwerdink, A. Tahraoui, C. Wenger, Y. Yamamoto, and P. V. Santos, Appl. Phys. Lett. **105**, 161904 (2014).
[24] F. C. Hsu, J. C. Hsu, T. C. Huang, C. H. Wang, and P. Chang, J. Phys. D: Appl. Phys. **44**, 375101 (2011).
[25] Z. Qiang, W. Zhou, and R. A. Soref, Opt. Express **15**, 1823 (2007).
[26] Y. Pennec, J. O. Vasseur, B. Djafari-Rouhani, L. Dobrzynski, and P. A. Deymier, Surf. Sci. Rep. **65**, 229 (2010).
[27] A. Salmana, O. A. Kaya, and A. Cicek, Sens. Actuat. A **208**, 50 (2014).
[28] A. Khelif and A. Adibi, *Phononic Crystals: Fundamentals and Applications* (Springer, New York, 2016).
[29] G. Mur, IEEE Trans. Electron. Comput. **EMC-23**, 377 (1981).
[30] R. K. Ameta, M. Singh, and R. K. Kale, J. Chem. Thermodyn. **60**, 159 (2013).
[31] S. Amoudache, Y. Pennec, B. Djafari Rouhani1, A. Khater, R. Lucklum, and R. Tigrine, J. Appl. Phys. **115**, 134503 (2014).
[32] D. R. Lide, *CRC Handbook of Chemistry and Physics*, Vol. 85, (CRC, Boca Raton, FL, 2004).